I&EC research
Industrial & Engineering Chemistry Research

Article

pubs.acs.org/IECR

Magnetic $CoFe_2O_4$–Graphene Hybrids: Facile Synthesis, Characterization, and Catalytic Properties

Yunjin Yao,*[,†,‡] Zeheng Yang,[†] Dawei Zhang,[†] Wenchao Peng,[‡,§] Hongqi Sun,[‡] and Shaobin Wang*[,‡]

[†]School of Chemical Engineering, Hefei University of Technology, Hefei 230009, P.R. China

[‡]Department of Chemical Engineering, Curtin University of Technology, GPO Box U1987, Perth, WA 6845, Australia

[§]School of Chemical Engineering and Technology, Tianjin University, Tianjin, 300072, P.R. China

ABSTRACT: This paper reports the synthesis of magnetic $CoFe_2O_4$–reduced graphene oxide (rGO) hybrids and the catalytic performance in heterogeneous activation of peroxymonosulfate (PMS) for decomposition of phenol. The surface morphologies and structures of the $CoFe_2O_4$–rGO hybrids were investigated by field emission scanning electron microscopy (SEM), energy-dispersive X-ray spectrometer (EDS), transmission electron microscopies(TEM), powder X-ray diffraction (XRD), Fourier transform infrared spectroscopy (FTIR), nitrogen adsorption–desorption isotherm, and thermogravimetric analysis (TGA). Through an in situ chemical deposition and reduction, $CoFe_2O_4$–rGO hybrids with $CoFe_2O_4$ nanoparticles of 23.8 nm were produced. Catalytic testing showed $CoFe_2O_4$–rGO hybrids exhibited much better catalytic activity than $CoFe_2O_4$, which suggests rGO plays an important role in $CoFe_2O_4$–rGO hybrids for the decomposition of phenol. Moreover, the hybrid catalyst presents good magnetism and could be separated from solution by a magnet.

1. INTRODUCTION

Graphene, a single layer of carbon atoms tightly packed into a two-dimensional honeycomb sp^2 carbon lattice, possesses a large surface area, open porous structure, flexibility, chemical stability, and very high electrical conductivity, which warrant it as a good candidate for constructing graphene-based composite materials with metal oxides.[1−3] Over the past decades, magnetic nanoparticles (NPs) have attracted intensive attention of many researchers because of their excellent physical and chemical properties compared with conventional bulk materials, such as superparamagnetism, high surface area, large surface-to-volume ratio, easy separation under external magnetic fields, and strong adsorption ability.[4−8] Nowadays, it is well realized that the dispersion of magnetic NPs on graphene sheets potentially becomes a hot topic of research due to their new and/or enhanced functionalities and therefore holds a great promise for a wide variety of applications in catalysis, biomedical fields, and removal of contaminants from wastewater.[9] With this in mind, graphene-based hybrids containing magnetic NPs have been recently reported.[10,11] We have reported the synthesis of magnetic Fe_3O_4@graphene composite and utilization in dye removal from aqueous media.[12] Li et al.[13] synthesized magnetic $CoFe_2O_4$-functionalized graphene nanocomposites by hydrothermal treatment of inorganic salts and thermal exfoliated graphene sheets as an effective absorbent for removing methyl orange in water.

Among various techniques of catalytic oxidation for water and wastewater treatment, Fenton reaction is one of the cost-effective technologies where hydroxyl radicals (•OH) are usually the main highly reactive oxidizing species generated to degrade organic contaminants. Similar to the activity of hydrogen peroxide, alternative oxidants such as peroxymonosulphate (PMS) have been found to be highly effective in chemically mineralizing various organic contaminants. Recently, cobaltous mediated peroxymonosulfate (Co/PMS) for degradation of contaminants has attracted interest and exhibited better efficiencies than the Fenton reaction in a wide pH range from 2 to 9.[14,15] However, the absence of practical and efficient approaches to recover the nanosized catalyst is a bottleneck for its environmental applications since nanosized materials, when discharged, might cause secondary environmental problems.[16] Magnetic cobalt ferrite ($CoFe_2O_4$), belonging to the family of spinel-type ferrites, has already been proposed for biomedical applications.[17] Recently, several attempts have been made using Co_3O_4 and $CoFe_2O_4$ as heterogeneous catalysts for activation of PMS.[14,18] The reaction mechanism for the degradation of phenol can be depicted as follows:[18,19]

$$Fe^{3+} + H_2O \leftrightarrow FeOH^{2+} + H^+ \quad (1)$$

$$Co^{2+} + FeOH^{2+} \leftrightarrow CoOH^+ + Fe^{3+} \quad (2)$$

$$CoOH^+ + HSO_5^- \leftrightarrow CoO^+ + SO_4^{-\bullet} \quad (3)$$

$$SO_4^{\bullet-} + \text{Phenol} \rightarrow [\text{...many steps...}] \rightarrow CO_2 + H_2O \quad (4)$$

The cobalt leaching from the Fe–Co catalysts can be controlled because of strong metal–metal interactions. Moreover, $CoFe_2O_4$ can be easily recovered using magnetic-based separation due to its ferromagnetic properties. Yang et al.[18] used ferromagnetic $CoFe_2O_4$ composites for the heterogeneous PMS activation and evaluated the catalyst performance in the degradation of highly toxic and poorly biodegradable 2,4-dichlorophenol. To the best of our knowledge, the preparation of $CoFe_2O_4$–graphene hybrids for the heterogeneous activation of PMS has not been reported.

Received: January 31, 2012
Revised: April 1, 2012
Accepted: April 9, 2012
Published: April 9, 2012

dx.doi.org/10.1021/ie300271p | *Ind. Eng. Chem. Res.* 2012, 51, 6044–6051

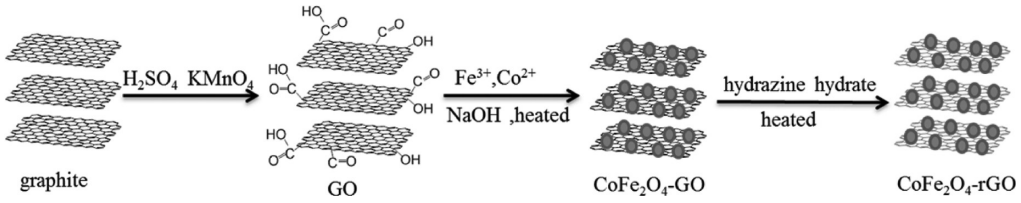

Figure 1. Preparation route of $CoFe_2O_4$–rGO.

In this paper, we present a facile approach for preparing $CoFe_2O_4$–reduced graphene oxide (rGO) via a chemical deposition of $CoFe_2O_4$ NPs onto GO, followed by reduction of GO to graphene in a hydrazine hydrate solution. The prepared materials were characterized by field emission scanning electron microscopy (FESEM), energy-dispersive X-ray spectrometer (EDS), transmission electron microscopies (TEM), powder X-ray diffraction (XRD), Fourier transform infrared spectroscopy (FTIR), nitrogen adsorption–desorption isotherm, and thermogravimetric analysis (TGA). The catalyst performance was evaluated in degradation of highly toxic and poorly biodegradable phenol, which is commonly used in different branches of industry.[20,21]

2. MATERIALS AND METHODS

2.1. Materials. Graphite powder (purity 99.9995%), iron-(III) nitrate nonahydrate (98%), sulphuric acid (95–97%), sodium hydroxide (50%), and potassium peroxymonosulfate ($2KHSO_5{\cdot}3KHSO_4{\cdot}3K_2SO_4$ available as Oxone, PMS) were obtained from Sigma-Aldrich. Hydrogen peroxide (30%) was purchased from Chem-Supply. Potassium permanganate and phenol were obtained from Ajax Finechem. Hydrazine hydrate (100%, synthesis grade) was obtained from Scharlau. Hydrochloric acid (32% analytical grade) and methanol (analytical grade) were obtained from Biolab. Cobalt nitrate hexahydrate was purchased from BDH/Merck.

2.2. Preparation of Magnetite $CoFe_2O_4$–rGO. GO was synthesized using the Hummers method through oxidation of graphite powder.[22,23]

For $CoFe_2O_4$–rGO synthesis, first, 0.9 g of GO was dispersed in 250 mL of water by sonication for 2 h to transform carboxylic acid groups to carboxylate anions. Then 1.72 g of $Fe(NO)_3{\cdot}9H_2O$ and 0.62 g of $Co(NO_3)_2{\cdot}6H_2O$ (molar ratio of Fe^{3+}/Co^{2+} as 2:1) were dissolved in 25 mL of water solution, which was added dropwise to GO solution at room temperature with vigorous stirring. After that 50% sodium hydroxide solution was added drop by drop to make solution pH >12 for synthesis of magnetite $CoFe_2O_4$ NP–GO. The temperature of the solution was raised to 80 °C and 10 mL of hydrazine hydrate was added with constant stirring for reduction of GO, resulting in a black solution. After being rapidly stirred for 5 h the solution was cooled to room temperature. The as-synthesized solid products were separated by centrifugation, washed thoroughly with water and absolute ethanol to remove any impurities, and then dried in a vacuum oven at 50 °C for 24 h.[24,25] Pure $CoFe_2O_4$ and rGO were obtained via the similar process in the absence of either GO or $CoFe_2O_4$. The synthesis process of the $CoFe_2O_4$–rGO hybrid is schematically illustrated in Figure 1.

2.3. Characterization. The crystallographic structure of the catalysts was investigated on a Bruker D8-Advance X-ray diffractometer with Cu Kα radiation (λ = 1.5418 Å), with accelerating voltage and current of 40 kV and 40 mA, respectively. FT-IR spectra were recorded on a Perkin-Elmer Spectrum 100 with a resolution of 4 cm^{-1} in transmission mode at room temperature. The morphology of the materials was characterized by FESEM (Zeiss Neon 40EsB FIBSEM) equipped with EDS and TEM (JEOL 2011 TEM). TGA was performed by heating the samples in an air flow at a rate of 100 mL/min using a Perkin-Elmer Diamond TG/DTA thermal analyzer with a heating rate of 10 °C/min. The surface area, total pore volume, and pore size distribution of all samples were determined by N_2 adsorption at −196 °C using Autosorb (Quantachrome Corp.). All samples were degassed at 100 °C for 4 h prior to the adsorption experiments. The Brunauer–Emmett–Teller (BET) surface area and pore volume were obtained by applying the BET equation and p/p_0 = 0.95 to the adsorption data, respectively. The pore size distribution was obtained by the Barrett–Joyner–Halenda (BJH) method.

2.4. Catalytic Oxidation. To study the activity of the catalytic oxidation of phenol, batch experiments were carried out in a 150-mL batch reactor. All reactions were initiated without the pH being controlled by mixing appropriate concentrations of phenol, oxone, and a catalyst. A fixed amount of oxone was added to a phenol solution and allowed to dissolve before the reaction. Later catalysts were added to start the reaction. The reaction was carried on for 1 h and stirred at different temperatures (25, 35, and 45 °C). Phenol was tested at four different initial concentrations ranging from 20 to 90 mg/L. Three different catalysts, rGO, $CoFe_2O_4$, and $CoFe_2O_4$–rGO, were also tested to investigate the effect of the different types of catalyst on the transformation of phenol. Oxone was also tested at several doses from 0.05 to 0.5 g. At predetermined time intervals, 0.5 mL of liquid was withdrawn using a syringe filter into a HPLC vial, and 0.5 mL of methanol was added to quench the reaction. The concentrations of phenol were analyzed using a HPLC with a UV detector at the wavelength of 270 nm. The column used was C-18 and the mobile phase was a solution of 30% CH_3CN and 70% water.[26,27]

3. RESULTS AND DISCUSSION

3.1. Characterization of Samples. The phase structure of as-synthesized samples was first determined by XRD. The XRD patterns of GO, $CoFe_2O_4$, and $CoFe_2O_4$–rGO are shown in Figure 2. The original GO sample shows a sharp peak at 2θ = 10.3° corresponding to the (001) reflection of GO. However, the characteristic peak of graphene oxide cannot be observed in the XRD pattern of $CoFe_2O_4$–rGO hybrids, and the X-ray diffraction peak of GO (100) crystal at 2θ = 42° totally disappears, suggesting GO was effectively reduced.[28] The diffraction peaks in Figure 2b can be perfectly indexed to the cubic spinel structure (JCPDS card 22-1086), and no characteristic peaks of impurities are detected in the XRD pattern, implying the formation of single-phase spinel.[29] As shown in Figure 2c, besides a weak peak appearing at 2θ = 26.5° corresponding to graphene, the XRD pattern of $CoFe_2O_4$–rGO is almost identical to that of $CoFe_2O_4$ NPs. Moreover, the

dx.doi.org/10.1021/ie300271p | Ind. Eng. Chem. Res. 2012, 51, 6044–6051

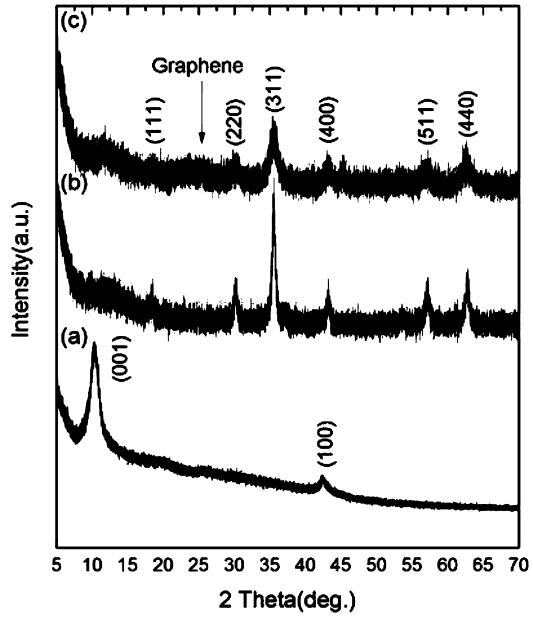

Figure 2. XRD patterns of (a) GO, (b) $CoFe_2O_4$, and (c) $CoFe_2O_4$–rGO.

observed diffraction peaks are broad and less sharp, indicating as-prepared $CoFe_2O_4$ with small dimensions. The average crystallite size of $CoFe_2O_4$ NPs can be estimated according to the diffraction reflections by using the Debye–Scherrer formula,[30] $D = 0.9\lambda/\beta \cos\theta$, where D is the average crystalline size, λ is the wavelength of Cu Kα, β is the full width at half-maximum (fwhm) of the diffraction peaks, and θ is the Bragg's angle. The average crystallite sizes were estimated to be 25.4 and 23.8 nm, respectively, for bare $CoFe_2O_4$ NPs and $CoFe_2O_4$ NPs in $CoFe_2O_4$–rGO.

FT-IR spectra of the various samples are shown in Figure 3. Several characteristic peaks of functional groups can be observed on GO, confirming the successful oxidation of graphite.

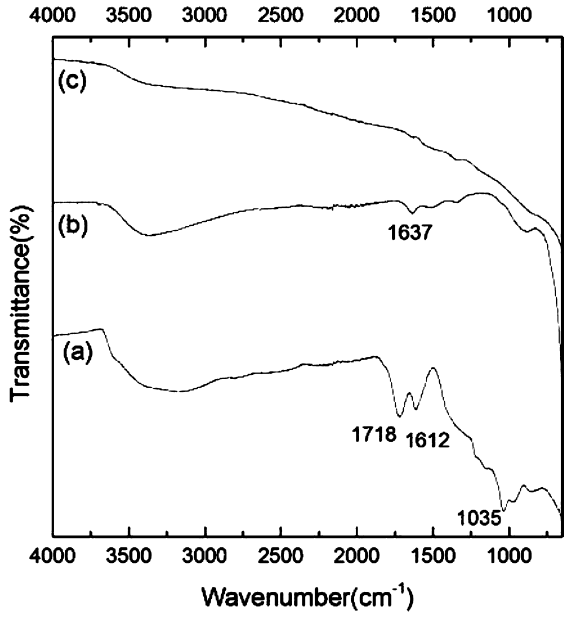

Figure 3. FTIR spectra of (a) GO, (b) $CoFe_2O_4$, and (c) $CoFe_2O_4$–rGO.

In detail, the peaks at 1718 and 1612 cm^{-1} should be assigned to the antisymmetric and symmetric stretching vibration of COO groups, and alkoxy C–O (1035 cm^{-1}) stretching vibrations were observed.[31] In contrast, most of the bands related with the oxygen-containing functional groups vanished in the FT-IR spectra (Figure 3c) of $CoFe_2O_4$–rGO. It is revealed that the bulk of the oxygen-containing functional groups were removed from GO in the process of reduction with hydrazine hydrate, and thus the GO was effectively transformed into graphene in the synthesis.[31] For the sample of $CoFe_2O_4$ in Figure 3b, the peak at 1637 cm^{-1} was ascribed to the vibration of adsorbed water.

To investigate the morphology and structure of the products, FESEM and TEM images were taken for the obtained $CoFe_2O_4$–rGO. The morphology of graphene is clearly visible from the FESEM and TEM images shown in Figure 4a, c, and $CoFe_2O_4$ NP were dispersed on the basal planes of the graphene. From Figure 4b, it can be observed that the graphene sheets are distributed between the packed $CoFe_2O_4$ NP and the nanoporous composite with a large amount of void space formed. Moreover, the graphene sheets distributed between the $CoFe_2O_4$ NP can prevent the aggregation of $CoFe_2O_4$ NP to a certain extent, which can be of great benefit to reactions. It also shows that the NPs are aggregated because of the magnetic dipolar interaction among the magnetite NPs. From Figure 4c the average particle size of $CoFe_2O_4$was determined to be as small as 25 nm, which is consistent with the average particle size calculated from the Scherrer's relation in X-ray diffraction pattern (23.8 nm). Furthermore, the composition of this structure is also confirmed by EDS spectroscopy (Figure 4d), which reveals the presence of Fe, Co, C, and O on the surfaces of the GO sheets (Al peak from the stub, and Pt peaks from the plated platinum). The atomic ratio of Fe to Co (19.3:9.7) is very close to the stoichiometric Fe/Co ratio in $CoFe_2O_4$, which further confirms the existence of $CoFe_2O_4$ NPs on graphene.

The specific surface area and pore volume of the samples were determined using the nitrogen sorption technique, with a typical isotherm shown in Figure 5. The isotherm demonstrates a type IV isotherm along with two small, but obvious, hysteresis loops at relative pressures of P/P_0 = 0.09 and 0.98, indicating the presence of interparticle and nonordered mesoporosity in the sample.[32] Furthermore, the pore size distribution of magnetic $CoFe_2O_4$–rGO was estimated to be about 1.7–5.9 nm by using the Barrett–Joyner–Halenda (BJH) analyses from the adsorption curve of the isotherm. Because the primary $CoFe_2O_4$ NPs are randomly packed, the pore size distribution of the product is not very uniform. The BET surface area and total pore volume were calculated to be 111.5 $m^2\ g^{-1}$ and 0.26 $cm^3\ g^{-1}$, respectively. These values are relatively large compared to pure $CoFe_2O_4$ structures. It is well-known that the theoretical specific surface area of graphene is as high as 2630 $m^2\ g^{-1}$.[33] However, the specific surface area of the graphene-based hybrid materials is much lower than the theoretical value due to the bigger weight contribution from NPs on the surface of graphene sheets.[34]

The content of each component in the prepared hybrids can be determined facilely with the TGA technique via oxidative decomposition. Figure 6 shows the representative TGA and DSC curves of GO and $CoFe_2O_4$–rGO, which were obtained in air atmosphere at a heating rate of 10 °C/min. Two samples showed a slight weight loss below 120 °C, ascribed to the evaporation of adsorbed water molecules. As shown in Figure 6a for GO, a slight weight loss occurs from 150 to 250 °C,

dx.doi.org/10.1021/ie300271p | Ind. Eng. Chem. Res. 2012, 51, 6044–6051

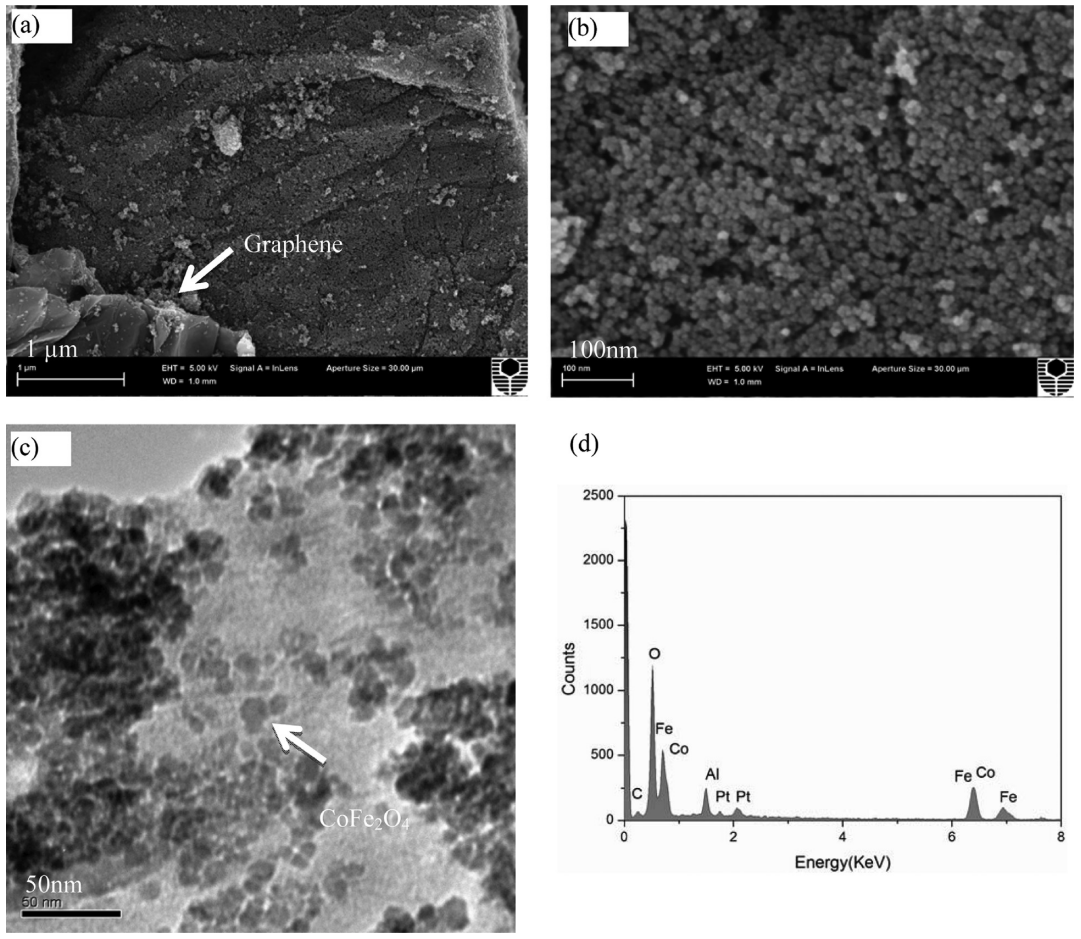

Figure 4. FESEM images (a: low-magnification, b: high-magnification) of $CoFe_2O_4$–rGO, (c) TEM, and (d) EDS of $CoFe_2O_4$–rGO.

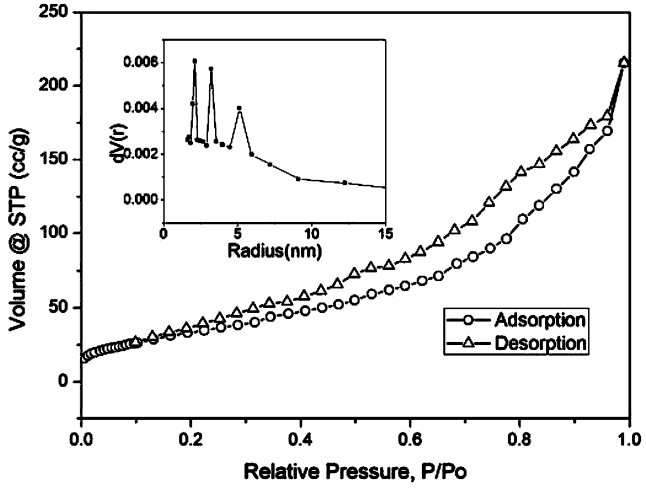

Figure 5. Nitrogen adsorption–desorption isotherm curve of the as-prepared $CoFe_2O_4$–rGO. Inset: pore size distribution.

which can be assigned to the removal of the labile oxygen-containing functional groups from the sample caused by the destruction of oxygenated functional groups.[35] Correspondingly, the DSC curve shows a strong exothermal peak centered at 207 °C. The final characteristic step/peak is in the range from 450 to 590 °C. Correspondingly, the DSC curve shows a strong exothermal peak centered at 535 °C. It can be assigned to the combustion and decomposition of carbon skeleton.[36]

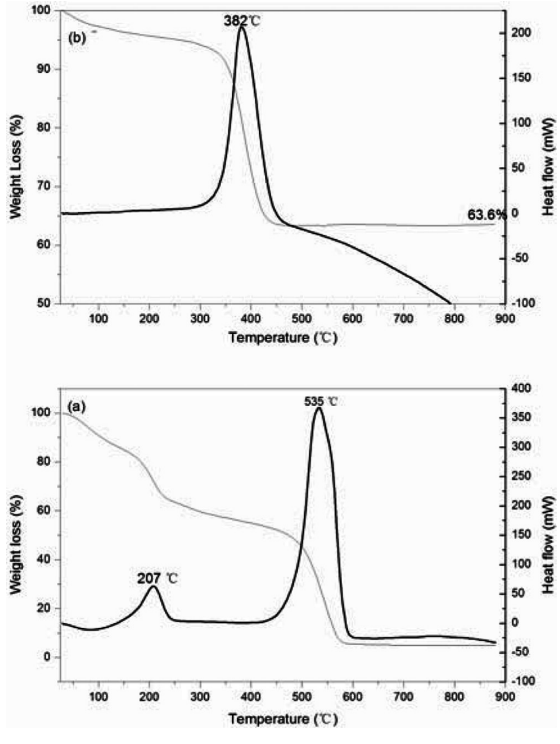

Figure 6. TG and DSC curves of (a) GO and (b) $CoFe_2O_4$–rGO in air atmosphere.

dx.doi.org/10.1021/ie300271p | *Ind. Eng. Chem. Res.* 2012, 51, 6044–6051

The TG/DSC curves of $CoFe_2O_4$–rGO present a characteristic step/peak in the range from 250 to 450 °C. Correspondingly, the DSC curve shows a strong exothermal peak centered at 382 °C, which is lower than GO. The lowering of the thermal decomposition temperatures of graphene (from 535 °C for GO to 382 °C for $CoFe_2O_4$–rGO) might be correlated to catalytic properties of the metal centers. When the temperature reached 450 °C, the weight of the sample remained and almost no further weight loss occurred after this temperature. According to the mass loss in $CoFe_2O_4$–rGO, about 63.6 wt % of metal oxide deposited on the surface of graphene, which was close to the starting ratio of GO and $CoFe_2O_4$.

Furthermore, $CoFe_2O_4$–rGO hybrids can be easily removed from the reaction media by applying an external magnetic field. $CoFe_2O_4$–rGO can be dispersed in the deionized water and forms a stable brown suspension before magnetic separation (Figure 7a).

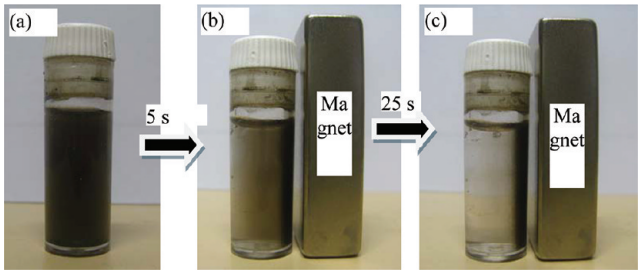

Figure 7. Photographs of the separation and redispersion processes of $CoFe_2O_4$–rGO: (a) without external magnetic field, and (b,c) with external magnetic field.

However, when a magnet was placed close to the reaction vessel for a while, it could be observed that the samples synthesized were rapidly attracted, and a nearly colorless solution was obtained (shown in Figure 7b, c). Therefore, the attraction and redispersion processes can be readily altered by switching an external magnetic field, showing good water-dispersion and magnetic separation characteristics of $CoFe_2O_4$–rGO in water solution.[12,37]

3.2. Catalytic Evaluation. The catalytic performances of $CoFe_2O_4$–rGO hybrid and individual components ($CoFe_2O_4$ and rGO) in the catalytic oxidation of phenol in the presence of PMS are shown in Figure 8. Nearly 23% of phenol (20 mg/L) was removed in 60 min in the presence of rGO, suggesting minor reaction of phenol degradation could occur. For $CoFe_2O_4$ sample, 51% of phenol was removed in 60 min. However, it was observed that the degradation rate of phenol with $CoFe_2O_4$–rGO was extremely fast and took around 30 min for complete phenol oxidation. Although rGO has less catalytic activity, $CoFe_2O_4$–rGO hybrids exhibited better catalytic activity than pure $CoFe_2O_4$, indicating that the catalytic activity of $CoFe_2O_4$ NPs can be remarkably improved by combining them with rGO sheets. This implies the crucial role of $CoFe_2O_4$ and rGO interactions on the $CoFe_2O_4$–rGO catalysts. Such an enhancement in catalytic activity can be attributed to three factors: (i) rGO has peculiar electronic structure and possesses high migration efficiency of electrons, which plays an important role in enhancing the catalytic activity for the degradation of phenol.[34] (ii) As compared with bare $CoFe_2O_4$ NPs, rGO can offer an environment to prevent aggregation of $CoFe_2O_4$ NPs and obstruct facile loss of activity. $CoFe_2O_4$–rGO hybrids have a higher surface area (111.5 $m^2\ g^{-1}$) than $CoFe_2O_4$ (56.0 $m^2\ g^{-1}$), which can provide more active sites for adsorption of reactants and catalytic decomposition of phenol. (iii) Graphene is not only a support, but also a catalyst for oxidation of phenol. Nevertheless, the novel properties of $CoFe_2O_4$–rGO as a catalyst lead us to believe that $CoFe_2O_4$–rGO hybrids will find application in various catalytic fields. The roles of the graphene and the reaction mechanism itself are still unclear and need further investigation.

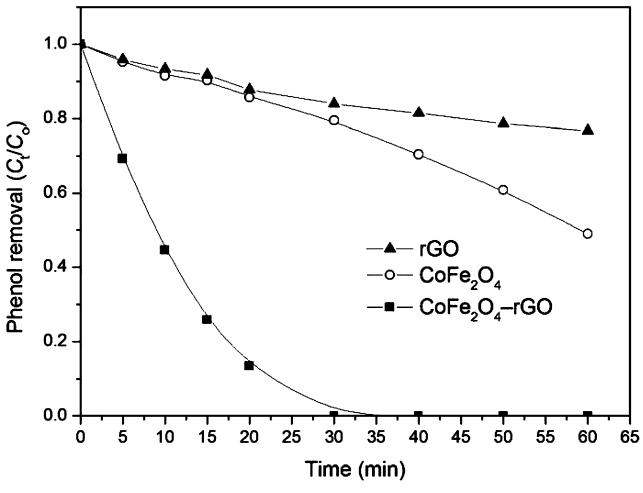

Figure 8. Phenol degradation using $CoFe_2O_4$–rGO/PMS. (Reaction conditions: [phenol] = 20 mg/L, [PMS] = 0.3 g/150 mL, [catalyst] = 10 mg/150 mL).

Figure 9 illustrates that upon increasing oxone dose (0.05, 0.1, 0.3, and 0.5 g), a faster and more efficient degradation of phenol occurred. It is also shown that increased doses of oxone led to the complete transformation time of 20 mg/L phenol from 45 to 30 min. The increase in PMS loading would provide more chance for the reaction with $CoFe_2O_4$–rGO, which enhances the rate of activation of PMS to generate active sulfate radicals, resulting in an increase in the rate of phenol removal.

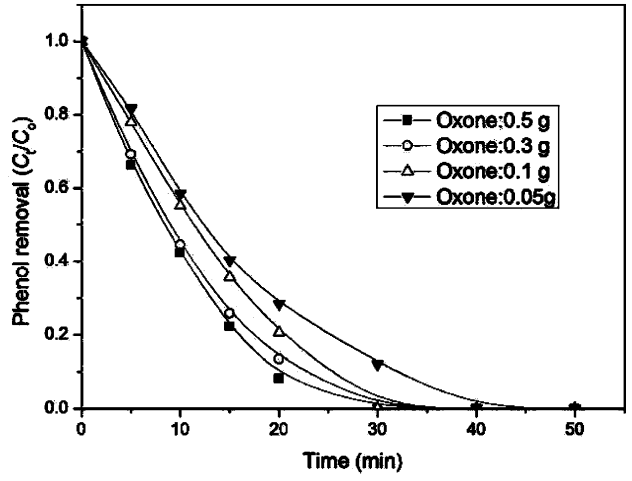

Figure 9. Phenol degradation using $CoFe_2O_4$–rGO/PMS: effect of oxone dose. (Reaction conditions: [phenol] = 20 mg/L, [catalyst] = 10 mg/150 mL).

Figure 10 shows that ultimate phenol removal efficiency decreased with decreasing initial phenol concentration (20, 40, 60, and 90 mg/L). The phenol in the reaction solution was almost completely removed within 60 min at the initial phenol concentration of less than 40 mg/L, while about 70% of phenol was removed within the same reaction time at the

dx.doi.org/10.1021/ie300271p | Ind. Eng. Chem. Res. 2012, 51, 6044–6051

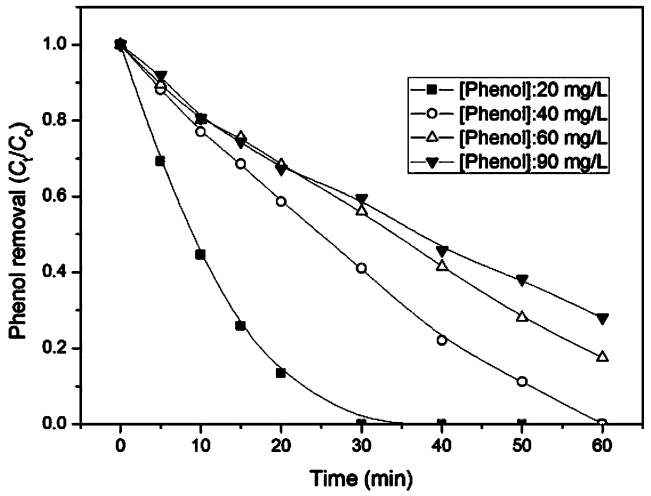

Figure 10. Phenol degradation using $CoFe_2O_4$–rGO/PMS: effect of phenol concentration. (Reaction conditions: [PMS] = 0.3 g/150 mL, [catalyst] = 10 mg/150 mL).

concentration of 90 mg/L. At the high phenol concentration, removal efficiency would be decreased.

Figure 11 compares the phenol degradation results obtained at varying temperatures of 25, 35, and 45 °C. As

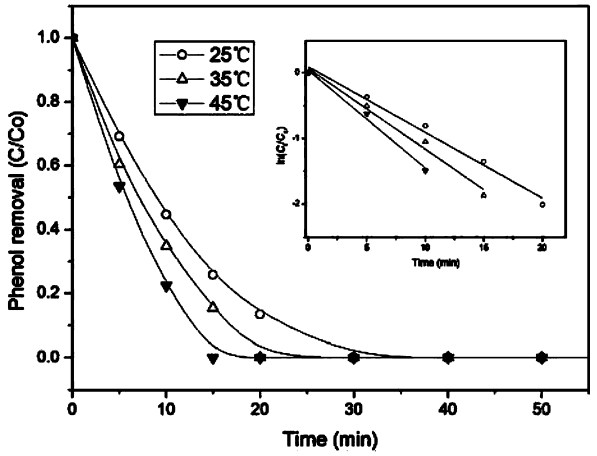

Figure 11. Phenol degradation using $CoFe_2O_4$–rGO/PMS: effect of temperature. Inset indicates kinetics of phenol degradation versus time. (Reaction conditions: [phenol] = 20 mg/L, [PMS] = 0.3 g/150 mL, [catalyst] = 10 mg/150 mL).

can be seen the rate of disappearance of phenol increased at increasing temperature. The kinetics of phenol conversion was evaluated by the first order model (inset of Figure 11) given in eq 5.

$$\ln\left(\frac{C_t}{C_0}\right) = k_{obs}t \tag{5}$$

where C_t and C_0 are the phenol concentrations at time (t) and $t = 0$, respectively, and k_{obs} is the rate constant. Accordingly, it was found that phenol degradation in $CoFe_2O_4$–rGO/PMS process is well formulated by the pseudo-first-order kinetics.[38] The pseudo-first-order rate constants (k_{obs}) of phenol degradation were found to be 0.1001 min^{-1} (R^2 = 0.982) at 25 °C, 0.1231 min^{-1} (R^2 = 0.979) at 35 °C, and 0.1494 min^{-1} (R^2 = 0.982) at 45 °C, (Table 1).

Table 1. Kinetic Rate Constants and Activation Energy of $CoFe_2O_4$–rGO/PMS Oxidation of Phenol

T, °C	k_{obs} (min^{-1})	R^2 of k_{obs}	ΔE (kJ mol^{-1})	R^2 of ΔE
25	0.1001	0.982	15.8	0.998
35	0.1231	0.979		
45	0.1494	0.982		

Based on the first-order kinetics, rate constants at varying temperatures were found to follow the Arrhenius equation.

$$k_{obs} = Ae^{-Ea/RT} \tag{6}$$

The factor A represents the frequency of collisions between two molecules in the proper orientation for reaction to occur. R is the gas constant, 8.314 J/(mol K), T is the temperature in Kelvin, and Ea is the activation energy. Ea was thus determined from the slope and intercept of the Arrhenius plot of ln (k_{obs}) versus $1/T$ (Figure 12).

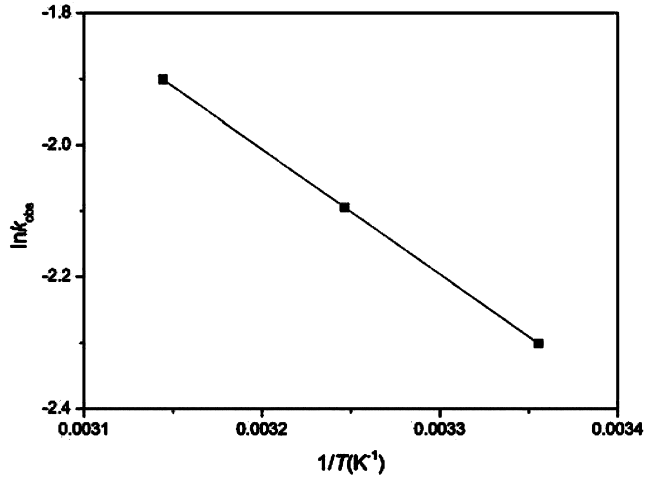

Figure 12. Arrhenius plot for the phenol degradation using $CoFe_2O_4$–rGO/PMS.

The activation energy was obtained as 15.8 kJ mol^{-1}, which is lower than the other Co materials in the references.[27] Considering its magnetic separation behavior and relatively high activity, $CoFe_2O_4$–rGO hybrids are promising catalytic materials for environmentally friendly oxidation processes.

4. CONCLUSION

Magnetic $CoFe_2O_4$–rGO hybrids were prepared by a chemical precipitation of Fe and Co precursors and reduction of GO in a hydrazine hydrate solution, characterized by FESEM, TEM, EDS, XRD, FTIR, and TGA techniques, and used for the degradation of phenol from aqueous solutions. $CoFe_2O_4$ NPs of size 23.8 nm were dispersed onto graphene sheets and $CoFe_2O_4$–rGO hybrids exhibited better catalytic activity than pure $CoFe_2O_4$. Phenol degradation on $CoFe_2O_4$–rGO followed the first order kinetics and activation energy is 15.8 kJ/mol. Considering their magnetic separation behavior and relatively high activity, $CoFe_2O_4$–rGO hybrids are environmentally friendly catalytic materials and recommended for further optimization and studies in relevant environmental applications.

dx.doi.org/10.1021/ie300271p | Ind. Eng. Chem. Res. 2012, 51, 6044–6051

AUTHOR INFORMATION

Corresponding Author

*Tel.: +86 551 2901458. Fax: +81 551 2901450. E-mail: yaoyunjin@gmail.com (Y.Y.). Tel.: +61 8 9266 3776. Fax: +61 8 9266 2681. E-mail: shaobin.wang@cutin.edu.au (S.W.).

Notes

The authors declare no competing financial interest.

ACKNOWLEDGMENTS

This work has been supported by the National Natural Science Foundation of China (NSFC Grants 20976033 and 21176054)

REFERENCES

(1) Yan, J.; Wei, T.; Qiao, W.; Shao, B.; Zhao, Q.; Zhang, L.; Fan, Z. Rapid microwave-assisted synthesis of graphene nanosheet/Co_3O_4 composite for supercapacitors. *Electrochim. Acta* **2010**, *55*, 6973−6978.

(2) Zhu, Y.; Murali, S.; Cai, W.; Li, X.; Suk, J. W.; Potts, J. R.; Ruoff, R. S. Graphene and graphene oxide: Synthesis, properties, and applications. *Adv. Mater.* **2010**, *22*, 3906−3924.

(3) Eda, G.; Chhowalla, M. Graphene patchwork. *ACS Nano* **2011**, *5*, 4265−4268.

(4) Gong, J.; Wang, B.; Zeng, G.; Yang, C.; Niu, C.; Niu, Q.; Zhou, W.; Liang, Y. Removal of cationic dyes from aqueous solution using magnetic multi-wall carbon nanotube nanocomposite as adsorbent. *J. Hazard. Mater.* **2009**, *164*, 1517−1522.

(5) Chen, L.; Xu, Z.; Dai, H.; Zhang, S. Facile synthesis and magnetic properties of monodisperse Fe_3O_4/silica nanocomposite microspheres with embedded structures via a direct solution-based route. *J. Alloys Compd.* **2010**, *497*, 221−227.

(6) Kaminski, M. D.; Nuñez, L. Extractant-coated magnetic particles for cobalt and nickel recovery from acidic solution. *J. Magn. Magn. Mater.* **1999**, *194*, 31−36.

(7) Chen, C.; Hu, J.; Shao, D.; Li, J.; Wang, X. Adsorption behavior of multiwall carbon nanotube/iron oxide magnetic composites for Ni(II) and Sr(II). *J. Hazard. Mater.* **2009**, *164*, 923−928.

(8) Imine, S.; Schoenstein, F.; Mercone, S.; Zaghrioui, M.; Bettahar, N.; Jouini, N. Bottom-up and new compaction processes: A way to tunable properties of nanostructured cobalt ferrite ceramics. *J. Eur. Ceram. Soc.* **2011**, *31*, 2943−2955.

(9) Zhang, Y.; Chen, B.; Zhang, L.; Huang, J.; Chen, F.; Yang, Z.; Yao, J.; Zhang, Z. Controlled assembly of Fe_3O_4 magnetic nanoparticles on graphene oxide. *Nanoscale* **2011**, *3*, 1446−1450.

(10) Lian, P.; Zhu, X.; Xiang, H.; Li, Z.; Yang, W.; Wang, H. Enhanced cycling performance of Fe_3O_4-graphene nanocomposite as an anode material for lithium-ion batteries. *Electrochim. Acta* **2010**, *56*, 834−840.

(11) Li, B.; Cao, H.; Shao, J.; Qu, M.; Warner, J. H. Superparamagnetic Fe_3O_4 nanocrystals@graphene composites for energy storage devices. *J. Mater. Chem.* **2011**, *21*, 5069−5075.

(12) Yao, Y.; Miao, S.; Liu, S.; Ma, L. P.; Sun, H.; Wang, S. Synthesis, characterization, and adsorption properties of magnetic Fe_3O_4@graphene nanocomposite. *Chem. Eng. J.* **2012**, *184*, 326−332.

(13) Li, N.; Zheng, M.; Chang, X.; Ji, G.; Lu, H.; Xue, L.; Pan, L.; Cao, J. Preparation of magnetic $CoFe_2O_4$-functionalized graphene sheets via a facile hydrothermal method and their adsorption properties. *J. Solid State Chem.* **2011**, *184*, 953−958.

(14) Chen, X.; Chen, J.; Qiao, X.; Wang, D.; Cai, X. Performance of nano-Co_3O_4/peroxymonosulfate system: Kinetics and mechanism study using Acid Orange 7 as a model compound. *Appl. Catal., B: Environ.* **2008**, *80*, 116−121.

(15) Chan, K. H.; Chu, W. Degradation of atrazine by cobalt-mediated activation of peroxymonosulfate: Different cobalt counteranions in homogenous process and cobalt oxide catalysts in photolytic heterogeneous process. *Water Res.* **2009**, *43*, 2513−2521.

(16) Hu, L.; Yang, X.; Dang, S. An easily recyclable Co/SBA-15 catalyst: Heterogeneous activation of peroxymonosulfate for the degradation of phenol in water. *Appl. Catal., B: Environ.* **2011**, *102*, 19−26.

(17) Cannas, C.; Musinu, A.; Ardu, A.; Orrù, F.; Peddis, D.; Casu, M.; Sanna, R.; Angius, F.; Diaz, G.; Piccaluga, G. $CoFe_2O_4$ and $CoFe_2O_4/SiO_2$ core/shell nanoparticles: Magnetic and spectroscopic study. *Chem. Mater.* **2010**, *22*, 3353−3361.

(18) Yang, Q.; Choi, H.; Al-Abed, S. R.; Dionysiou, D. D. Iron−cobalt mixed oxide nanocatalysts: Heterogeneous peroxymonosulfate activation, cobalt leaching, and ferromagnetic properties for environmental applications. *Appl. Catal., B: Environ.* **2009**, *88*, 462−469.

(19) Anipsitakis, G. P.; Dionysiou, D. D.; Gonzalez, M. A. Cobalt-mediated activation of peroxymonosulfate and sulfate radical attack on phenolic compounds. Implications of chloride ions. *Environ. Sci. Technol.* **2006**, *40*, 1000−1007.

(20) Gupta, V. K.; Sharma, S.; Yadav, I. S.; Mohan, D. Utilization of bagasse fly ash generated in the sugar industry for the removal and recovery of phenol and p-nitrophenol from wastewater. *J. Chem. Technol. Biotechnol.* **1998**, *71*, 180−186.

(21) Gupta, V. K.; Carrott, P. J. M.; Ribeiro Carrott, M. M. L. Suhas, Low-cost adsorbents: Growing approach to wastewater treatment—a review. *Crit. Rev. Environ. Sci. Technol.* **2009**, *39*, 783−842.

(22) Hartono, T.; Wang, S.; Ma, Q.; Zhu, Z. Layer structured graphite oxide as a novel adsorbent for humic acid removal from aqueous solution. *J. Colloid Interface Sci.* **2009**, *333*, 114−119.

(23) Bradder, P.; Ling, S. K.; Wang, S.; Liu, S. Dye adsorption on layered graphite oxide. *J. Chem. Eng. Data* **2010**, *56*, 138−141.

(24) Chandra, V.; Park, J.; Chun, Y.; Lee, J. W.; Hwang, I.-C.; Kim, K. S. Water-dispersible magnetite-reduced graphene oxide composites for arsenic removal. *ACS Nano* **2010**, *4*, 3979−3986.

(25) Li, B.; Cao, H.; Shao, J.; Li, G.; Qu, M.; Yin, G. Co_3O_4@graphene composites as anode materials for high-performance lithium ion batteries. *Inorg. Chem.* **2011**, *50*, 1628−1632.

(26) Hardjono, Y.; Sun, H.; Tian, H.; Buckley, C. E.; Wang, S. Synthesis of Co oxide doped carbon aerogel catalyst and catalytic performance in heterogeneous oxidation of phenol in water. *Chem. Eng. J.* **2011**, *174*, 376−382.

(27) Sun, H.; Tian, H.; Hardjono, Y.; Buckley, C. E.; Wang, S. Preparation of cobalt/carbon-xerogel for heterogeneous oxidation of phenol. *Catal. Today* **2011**, No. http://dx.doi.org/10.1016/j.cattod.2011.09.001.

(28) Huang, X.; Zhao, X.; Wang, Z.; Wang, L.; Zhang, X. Facile and controllable one-pot synthesis of an ordered nanostructure of $Co(OH)_2$ nanosheets and their modification by oxidation for high-performance lithium-ion batteries. *J. Mater. Chem.* **2012**, *22*, 3764−3769.

(29) Ai, L.; Huang, H.; Chen, Z.; Wei, X.; Jiang, J. Activated carbon/$CoFe_2O_4$ composites: Facile synthesis, magnetic performance and their potential application for the removal of malachite green from water. *Chem. Eng. J.* **2010**, *156*, 243−249.

(30) Jiang, H. G.; Ruhle, M.; Lavernia, E. J. On the applicability of the X-ray diffraction line profile analysis in extracting grain size and microstrain in nanocrystalline materials. *J. Mater. Res.* **1999**, *14*, 549−559.

(31) Ji, Z.; Shen, X.; Song, Y.; Zhu, G. In situ synthesis of graphene/cobalt nanocomposites and their magnetic properties. *Mater. Sci. Eng., B* **2011**, *176*, 711−715.

(32) Xuan, S.; Wang, F.; Lai, J. M. Y.; Sham, K. W. Y.; Wang, Y.-X. J.; Lee, S.-F.; Yu, J. C.; Cheng, C. H. K.; Leung, K. C.-F. Synthesis of biocompatible, mesoporous Fe_3O_4 nano/microspheres with large surface area for magnetic resonance imaging and therapeutic applications. *ACS Appl. Mater. Interfaces* **2011**, *3*, 237−244.

(33) Ning, G.; Fan, Z.; Wang, G.; Gao, J.; Qian, W.; Wei, F. Gram-scale synthesis of nanomesh graphene with high surface area and its application in supercapacitor electrodes. *Chem. Commun.* **2011**, *47*, 5976−5978.

(34) Ji, Z.; Shen, X.; Zhu, G.; Zhou, H.; Yuan, A. Reduced graphene oxide/nickel nanocomposites: Facile synthesis, magnetic and catalytic properties. *J. Mater. Chem.* **2012**, *22*, 3471−3477.

(35) Xu, C.; Wang, X.; Zhu, J.; Yang, X.; Lu, L. Deposition of Co_3O_4 nanoparticles onto exfoliated graphite oxide sheets. *J. Mater. Chem.* **2008**, *18*, 5625−5629.
(36) Wang, J.; Zheng, S.; Shao, Y.; Liu, J.; Xu, Z.; Zhu, D. Amino-functionalized Fe_3O_4@SiO_2 core-shell magnetic nanomaterial as a novel adsorbent for aqueous heavy metals removal. *J. Colloid Interface Sci.* **2010**, *349*, 293−299.
(37) Hui, C.; Shen, C.; Tian, J.; Bao, L.; Ding, H.; Li, C.; Tian, Y.; Shi, X.; Gao, H.-J. Core-shell Fe_3O_4@SiO_2 nanoparticles synthesized with well-dispersed hydrophilic Fe_3O_4 seeds. *Nanoscale* **2011**, *3*, 701−705.
(38) Huang, Y.-F.; Huang, Y.-H. Behavioral evidence of the dominant radicals and intermediates involved in Bisphenol A degradation using an efficient Co^{2+}/PMS oxidation process. *J. Hazard. Mater.* **2009**, *167*, 418−426.